Correlative nano-imaging of metals and proteins in primary neurons by synchrotron X-ray fluorescence and STED super resolution microscopy: experimental validation

Richard Ortega[a], Stéphane Roudeau[a], Asuncion Carmona[a*]

[a] Univ. Bordeaux, CNRS, LP2I Bordeaux, UMR 5797, Chemical Imaging and Speciation, F-33170 Gradignan, France

Keywords: Neuron, Imaging, Metals, Cytoskeleton, Synchrotron, X-ray fluorescence, Super resolution

*Corresponding author at: Univ. Bordeaux, CNRS, LP2I Bordeaux, Chemical Imaging and Speciation, F-33170 Gradignan, France

Email address: Asuncion Carmona asuncion.carmona@u-bordeaux.fr

ABSTRACT

Background: It is becoming increasingly clear that biological metals such as iron, copper or zinc are involved in synaptic functions, and in particular in the mechanisms of synaptogenesis and subsequent plasticity. Understanding the role of metals on synaptic functions is a difficult challenge due to the very low concentration of these elements in neurons and to the submicrometer size of synaptic compartments.

New method: To address this challenge we have developed a correlative nano-imaging approach combining metal and protein detection. First, stimulated emission depletion (STED) microscopy, a super resolution optical microscopy technique, is applied to locate fluorescently labeled proteins. Then, synchrotron radiation induced X-ray fluorescence (SXRF) is performed on the same regions of interest, e.g. synaptic compartments.

Results: We present here the principle scheme that allows this correlative nano-imaging and its experimental validation. We applied this correlative nano-imaging to the study of the physiological distribution of metals in synaptic compartments of primary rat hippocampal neurons. We thus compared the nanometric distribution of metals with that of synaptic proteins, such as PSD95 or cytoskeleton proteins.

Comparison with existing method(s): Compared to correlative imaging approaches currently used to characterize synaptic structures, such as electron microscopy correlated with optical fluorescence, our approach allows for ultra-sensitive detection of trace metals using highly focused synchrotron radiation beams.

Conclusion: We provide proof-of-principle for correlative imaging of metals and proteins at the synaptic scale and discuss the present limitations and future developments in this area.

1. Introduction

Metals essential to life such as manganese (Mn), iron (Fe), copper (Cu) or zinc (Zn) are required in many biological processes, including neurobiological functions and their dyshomeostasis is involved in neurodegeneration (Wandt et al., 2021). The study of the biological functions of these metals in neurons remains nevertheless a challenge because their concentration in biological samples is low, and the nature of interactions with biological molecules is often labile. Thus, the imaging of metals at the scale of neuronal structures requires the implementation of analytical methods of very high sensitivity, high spatial resolution, combined to non-denaturating sample preparation methods (White, 2017).

Synchrotron radiation induced X-ray fluorescence (SXRF) imaging is a method well suited to investigate the distribution of metals in the brain (White, 2017; Finnegan et al., 2019; Ellison et al., 2022). SXRF technique gives access to the total content of the elements, which includes for example both labile and bounded metals. SXRF can be performed at nanometric spatial resolution to explore synaptic compartments in neurons (Perrin et al., 2017). In order to derive relevant information from SXRF nano-imaging experiments it is nevertheless necessary to optimize experimental parameters as will be discussed in this article. In particular, we have studied the possibility of comparing the distribution of biological metals with that of proteins of interest, in order to understand the physiological functions of metals. We have developed a methodological workflow combining nano-SXRF imaging and STED (stimulated emission depletion) super resolution fluorescence microscopy applied to the correlative imaging of metals and proteins in cultured primary rat hippocampal neurons (Domart et al., 2020; Carmona et al., 2022). This approach includes maintaining the native distribution of these elements in neuronal compartments. The aim of this article is to present the sample preparation issues to face this challenge and to show results of experimental validation, to discuss future improvements.

Concerning the validation of the correlative nano-imaging approach we checked experimentally the possibility to analyze the same regions of interest by both nano-imaging methods, SXRF and STED. We verified the correct superposition of chemical element and protein images at the level of sub-synaptic compartments. With respect to preservation of cell morphology and native subcellular distribution of chemical elements, we have opted for a protocol based on the use of cryogenic methods of sample preparation based on cryofixation and freeze-drying. These sample preparation methods also have limitations in terms of morphological preservation, but are essential to preserve the distribution of chemical elements. We will discuss possible evolutions to further improvements of these protocols.

2. Material and methods

2.1. Cell culture

Freshly isolated embryonic primary hippocampal neurons from E18 Sprague-Dawley rats were used. Neurons were cultured directly on silicon nitride (SN) membranes in order to perform synchrotron X-ray spectro-microscopy. We used SN membranes with silicon frame of 5 mm x 5 mm side, and a frame thickness of 200 µm, with at the center a SN membrane of 1.5 mm x 1.5 mm side and a thickness of 500 nm (Silson, UK). The SN membranes were designed with a marking on the outer edge that serves as a reference for orientation.

The culture of primary neurons on the SN membranes was adapted from protocols to culture neurons on glass coverslips (Kaech & Banker, 2006; Domart et al., 2020). First, the SN membranes are sterilized with high grade ethanol for 1.5 hour and allowed to dry for two hours. Then they are treated with an adhesion factor, poly-L-lysine. We soak the membranes in poly-L-lysine for 2.5 h and then remove it and add culture medium, leave them at 37°C until use, 2-3 days later. On the day of seeding, the neurons are spread on the membranes at an homogeneous density of 20,000 neurons per cm^2, and left for two hours in the incubator at 37°C. After this time the membranes are transferred to a culture plate containing a layer of glial cells. Neurons can be used at different DIV (day in vitro) depending on the purpose of the study. For example, we investigated neurobiology of metals in growth cones at DIV3 on the one hand and in dendritic spines at DIV15 on the other hand.

2.2. Fluorescent labeling of proteins

Two approaches were applied for the fluorescence imaging of proteins. We transfected primary neurons with a plasmid coding for Xph20-eGFP, a fluorescent molecular construct designed to bind the postsynaptic scaffold protein PSD-95 (Rimbault et al., 2021). The second method is the direct labeling of tubulin and/or F-actin with silicon-rhodamine (SiR) dyes designed for STED microscopy (Lukinavičius, 2016). For the transfection, primary neurons were electroporated at DIV0 with the plasmid Xph20-eGFP, then plated on SN membranes. In this case, twice as many neurons are plated (40,000 neurons/cm^2) compared to cultures without transfection to compensate for a lower number of neurons adhering to the SN membranes. Neurons were electroporated by Nucleofector® Technology, using a 4D-NucleofectorTM device, a P3 Primary cell solution Kit (Lonza) using 3 µg of DNA per 300,000 neurons following the protocol given by Lonza and the high viability program.

The other approach consisted in a direct labeling using SiR-tubulin and SiR700-actin fluorophores (Spirochrome). In this case, DIV3 neurons for growth cone studies, or DIV15 neurons for dendritic spine studies cultured on SN membranes were removed from the astrocyte culture plate and exposed to 1 µM of the probes diluted in culture medium for 1 hour at 37°C following instructions from Spirochrome manufacturer. The labeling is done just before observation to limit the decrease in fluorescence intensity over time.

2.3. STED and confocal microscopy

Confocal and STED microscopy were performed on live neurons with the same inverted microscope, a Leica DMI6000 SP8 X. To observe living cells in the Ludin chamber, SN membranes are placed with the cells facing the objective. We performed dual color microscopy by combining SiR-tubulin with SiR700-actin or with Xph20-eGFP. Excitation was conducted with a white light laser 470-670 nm settled at 640 nm (for SiR fluorophores) or 488 nm for GFP. The emission was recorded using a Leica HyD detector (hybrid detector) within the following spectral ranges 650-700 nm for SiR, 720-770 nm for SiR700 and 492-561 nm for GFP. For STED acquisition a 775 nm depletion laser was used. To analyze the same neuron by STED and SXRF, the relative position of the selected neurons is determined with respect to the corners of the silicon frame of the SN membrane and using the orientation marker. The microscope allows to record, for each analysis, the position of the microscope with respect to the sample-stage. Thus, the positions of each imaged neuron and the positions of each membrane edge with respect to the sample stage are recorded. After the STED microscopy, a transformation of the reference system is performed to calculate the new coordinates on the SXRF microscope.

2.4. Sample preparation for SXRF analysis

Samples were prepared for SXRF analysis by plunge-freezing and freeze-drying. The structure and chemical element distribution of neurons can be preserved using this cryo-processing approach (Perrin et al., 2015; Perrin et al., 2017; Carmona et al., 2022). In brief, after live-cell microscopy, samples were washed with an ammonium acetate buffer solution adjusted to pH 7.4 and 240 mOsm prepared with ultra trace elemental analysis grade water (Fisher Scientific). This washing removes the remaining salts from the Tyrode's solution from the surface of the samples. After washing, excess ammonium acetate solution was blotted by capillarity from the edges of the membrane, avoiding contact with neurons, with ultra-absorbent paper (Whatman). Then the samples were rapidly immersed in liquid methylbutane that had been chilled down to -156°C with liquid nitrogen. The excess of methylbutane on the SN membranes was absorbed with ultra-absorbent filter paper after plunge-freezing, keeping the samples immersed in liquid nitrogen vapors during all the process. After plunge freezing, the samples were freeze-dried at -75°C for 48 hours under a primary vacuum (2.10^{-3} mbar) using a Christ alpha 2-4 LD plus freeze-dryer.

2.5. Scanning electron microscopy

In order to verify the cell morphology preservation of cultured neurons after cryofixation and freeze-drying, scanning electron microscopy (SEM) was performed at the electron microscopy unit of Bordeaux Imaging Center, with a Zeiss GeminiSEM300 using a 1 kV accelerating voltage. SN membranes with cryofixed and freeze-dried neurons as prepared for SXRF imaging were introduced in the vacuum chamber of the microscope and observed at different magnifications, from low magnification (x660) to identify neuronal cell bodies, to high spatial resolution (x10,000) to observe thin dendritic structures.

2.6. SXRF nano-imaging

This experimental validation study presents the results of SXRF analyses performed on two different facilities, the ESRF ID16A Nano-Imaging beamline (Da Silva et al., 2017), and the Bionanoprobe at Argonne National Laboratory's Advanced Photon Source (APS) (Chen et al., 2014).

At ID16 Nano-Imaging beamline, a pair of multilayer-coated Kirk-Patrick Beaz mirrors that are 185 m downstream of the undulator source is used to focus the incident X-ray at the energy of 17 keV. The freeze-dried specimens were measured under a vacuum of 1.10^{-7} mbar. Regions of interest were raster-scanned with a beam focal spot of 35 x 57 nm^2, with a flux of 4.10^{11} photons/s, a dwell time of 200 ms and a step size of 40 nm. The sample was placed in normal incidence and a 6-elements silicon drift detector (SGX Sensortech, UK) was aligned within the X-ray focal plane, and located perpendicular to the beam path on the side of the sample to collect the fluorescence signals. The summed spectra from the multi-element detectors were fitted by PyMca software (Solé et al., 2007) against the signal derived from a thin film X-ray fluorescence standard (AXO Dresden GmbH, Germany) to obtain quantitative maps of the element distributions.

At the Bionanoprobe beamline, Fresnel zone plates were used to focus 10 keV monochromic X-ray photons on the samples. The pixel size ranged from 85 to 200 nm, with a flux of 10^9 photons/s and a maximum integration time of 2 seconds per pixel. A full X-ray fluorescence spectra was collected at each pixel as the sample was raster scanned across the incident X-ray beam using a 4-elements silicon drift detector (Vortex ME4, Hitachi High-Technologies Science America). The spectra were then fitted and quantified using MAPS software against a standard thin film (RF8-200-S2453, AXO Dresden GmbH) measured in the same conditions (Vogt et al., 2003).

3. Results and discussion

3.1. Overview of the main steps of the correlative nano-imaging protocol.

The methodological workflow developed to correlate STED super resolution microscopy of fluorescently labeled proteins with SXRF mapping of biological metals in cultured primary neurons is schematically represented in Fig. 1. The first step consists of culturing the neurons on SN membranes, which are thin and transparent supports compatible for both STED and SXRF imaging (Domart et al., 2020; Carmona et al., 2022). The next step is to label the proteins of interest with fluorophores using molecules adapted to live cell imaging. The third step consists of performing STED microscopy of fluorescently labeled proteins on living neurons and determining their positions with respect to the membrane edges in order to further perform image correlation. Thanks to the STED super resolution microscopy, the distribution of the proteins of interest is determined with spatial resolutions of the order of tens of nanometers (Choquet et al., 2021). For our correlative approach one of the advantages of STED microscopy is that it can be performed on living cells, without the need to perform chemical fixation known to modify elemental distributions (Roudeau et al., 2014; Perrin et al., 2015; Jin et al., 2017), and cellular nanostructure (Li et al., 2017). The fourth step refers to sample preparation, once the regions of interest are captured by STED microscopy, samples are immediately plunge frozen at low temperature to avoid elemental redistribution, and freeze-dried also at low temperature. The fifth and final step is to perform SXRF spectro-imaging on beamlines that provide nanometric spatial resolution, comparable to STED resolution. Finally, STED and SXRF images are obtained on the same regions of interest and with similar spatial resolution allowing for the direct correlation of proteins and biological metals.

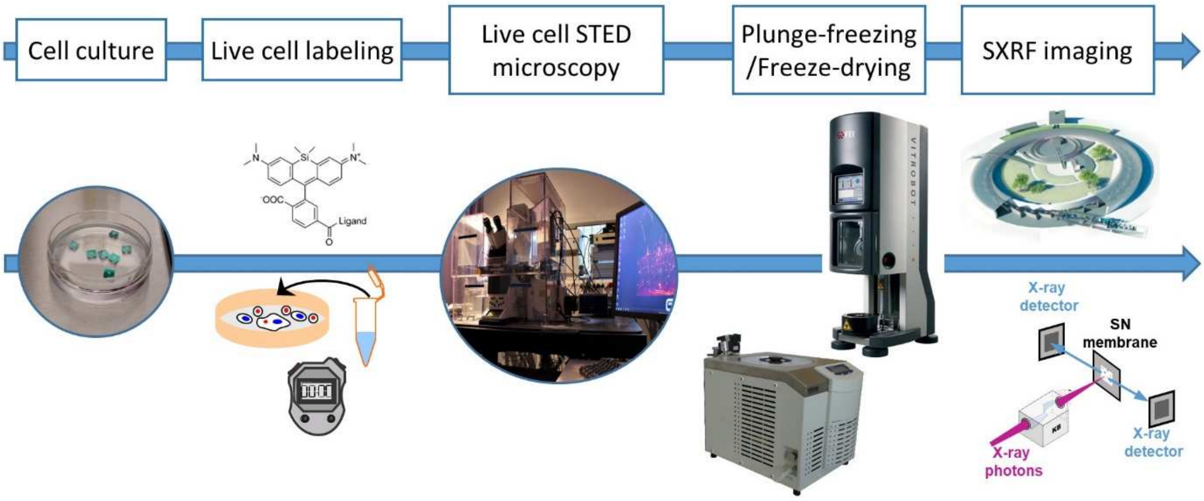

Fig. 1. Schematic representation of the different steps required for STED/SXRF correlative nano-imaging. First, primary neurons are cultured onto SN membranes and the proteins of interest are labeled with fluorophores designed for STED microscopy. Fluorescently labeled proteins are localized in cultured neurons using live-cell STED microscopy. Samples are immediately plunge frozen and freeze-dried to preserve the chemical element distribution. Finally, multi-elemental mapping is performed using SXRF nano-imaging on the same regions of interest previously identified by STED microscopy.

3.2. Validation of the image overlay

For correlative microscopy it is essential to observe the same regions of interest on the sample which can be difficult to achieve when the imaging methods are implemented on different instruments, in this case the STED microscope and the synchrotron radiation beamline. In our case we have opted for a simple image recognition pattern consisting in the overlay of STED and SXRF images based first on an coordinate measurement to locate the regions of interest relatively to the orientation marker of the membrane, followed by a finer correlation relying on specific structures identified on both STED and SXRF images (Domart et al., 2020). An example of correlation between proteins and chemical elements in dendritic areas of hippocampal neurons is shown in Fig. 2. Tubulin and F-actin were labeled with SiR-tubulin and SiR-700-actin to perform dual color confocal and STED microscopy using the Leica DMI6000 SP8 X microscope on living neurons (Fig. 2A and 2D respectively). The same region of interest was imaged at the nano-imaging beamline ID16A at ESRF (Fig. 2G). Although STED microscopy is performed on living neurons and SXRF on subsequently cryofixed and freeze-dried samples, the morphology is well preserved and both images can be superimposed (Fig. 2E). It is also important for the correlative microscopy purpose that the images from the different techniques are obtained with a similar spatial resolution to allow a relevant superposition of the images. This is exemplified in Fig. 2F, where it can be seen that confocal microscopy cannot resolve the two thin dendrites in the analyzed area (Fig. 2B) whereas they can be distinguished by STED (Fig. 2C) and by SXRF (Fig. 2E). Some elements such as Fe and Cu are below the detection limit in these very thin dendrites (Fig. 2G). In addition, it is noteworthy that SXRF imaging reveals the appearance of structures on the thin dendrites that are not observed by protein fluorescence microscopy, because these structures do not content the labeled proteins or because the protein labeling is not 100% efficient.

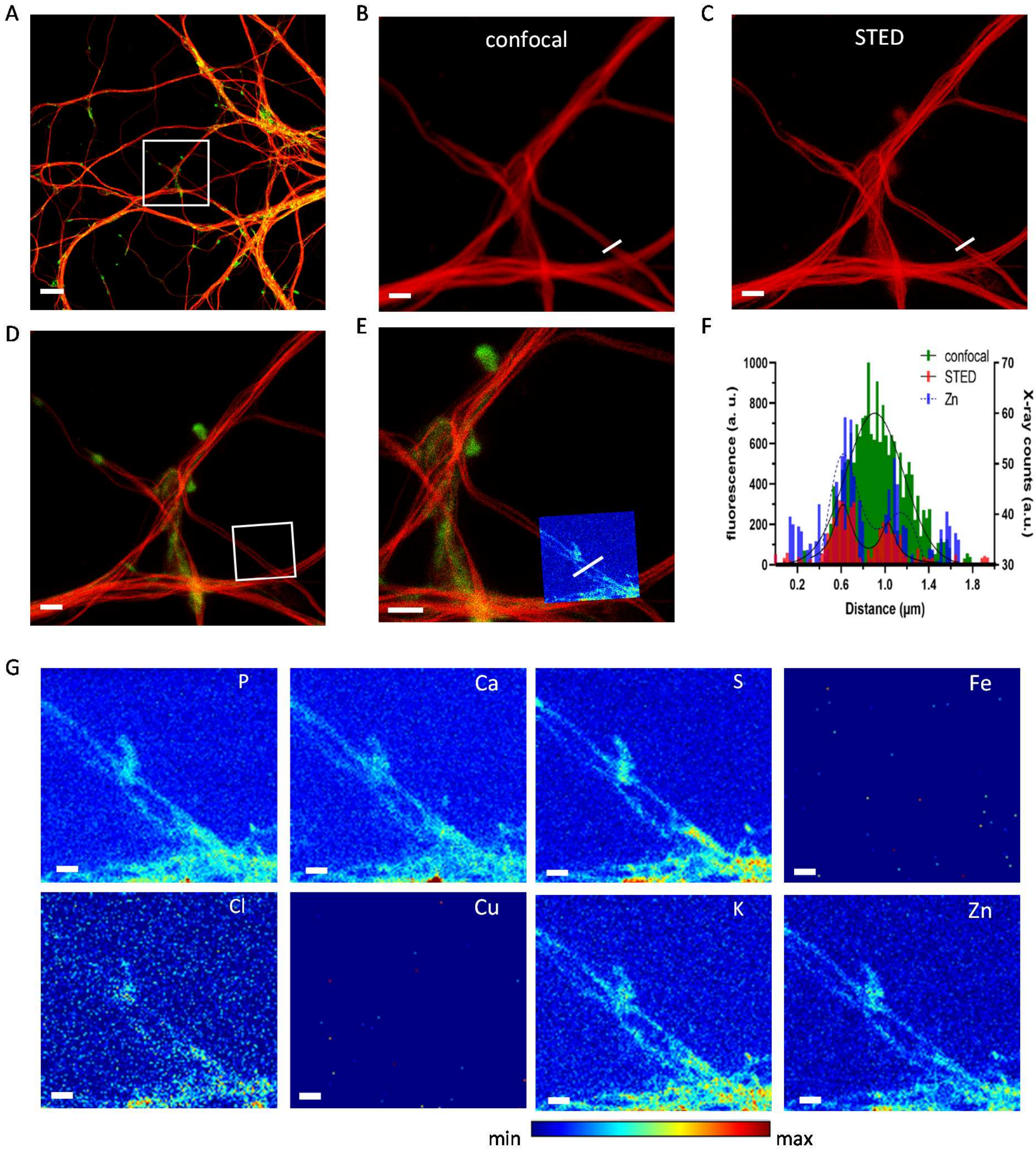

Fig. 2. Correlation of STED microscopy and nano-SXRF images obtained at ID16A beamline (ESRF) in dendrites. (A) Confocal microscopy view of tubulin (red, labeled with SiR-tubulin) and F-actin (green, labeled with SiR-700-actin) in living cells. (B) Live-cell confocal microscopy images of tubulin from the white square region in A. (C) Live-cell STED microscopy of tubulin in the same area as B showing the higher resolving power of STED *vs* confocal microscopy. (D) Live-cell STED microscopy images of tubulin (red) and F-actin (green) corresponding to the white square region in A. (E) Merged images of STED microscopy in living cells (tubulin and actin) and SXRF mapping in freeze-dried cells (Zn map). (F) Plot profile intensities across the white line labeled in B, C and E to compare confocal, STED and SXRF spatial resolution. (G) SXRF images of chemical elements from the white square region in D, after plunge freezing and freeze-drying. Color scale bar: min-max values. Scale bars: (A) 10 µm, (B, C, D, E) 2 µm, (G) 0.5 µm.

3.3. Validation of element content preservation

The most commonly used sample preparation methods for fluorescent protein imaging are based on chemical fixation of proteins with aldehydes. However, this chemical fixation causes permeabilization of biological membranes and drastic losses of intracellular elements, including biological metals (Roudeau et al., 2014; Perrin et al., 2015; Jin et al., 2017). This is why we opted for a live-cell microscopy of fluorescent proteins and probes followed by a cryogenic fixation by fast plunge freezing which allows an excellent structural preservation, in particular of proteins, while preserving the distribution of chemical elements (Domart et al., 2020). However, it is not known whether the protocol of labeling proteins with fluorophores designed for STED microscopy does not cause changes in the distribution of chemical elements. For this reason, we compared SXRF analyses of neurons labeled with SiR-tubulin and SiR700-actin molecules with those of neurons in their native, not labeled, state (Fig. 3). Comparing the images corresponding to fluorescently labeled (Fig. 3A) and unlabeled growth cones (Fig. 3B), we observe that the distribution of the elements is similar in both cases. This result is confirmed by comparing the individual SXRF spectra of multiple analyses (Fig. 3C). SXRF spectra corresponding to 5 individual growth cones from unlabeled samples (blue dotted lines) and from 8 individual growth cones labeled with SiR-tubulin and SiR-actin (red dotted lines) are plotted In Fig. 3C. Individual spectra were normalized to the Si signal coming from the SN membrane, which can be used here as internal standard. The number of X-ray counts is proportional to the thickness of the growth cone, which can slightly vary, explaining the small differences between the spectra. For ease of comparison, we have plotted, as solid line, the mean spectrum for each group. The mean SXRF spectrum corresponding to the unlabeled samples, in blue, is comparable with the one of labeled samples, in red (Fig. 3C). It can be concluded that the STED fluorophores do not induce significant changes in elemental content. Only a slight decrease of Ca content, a highly diffusible element, is observed.

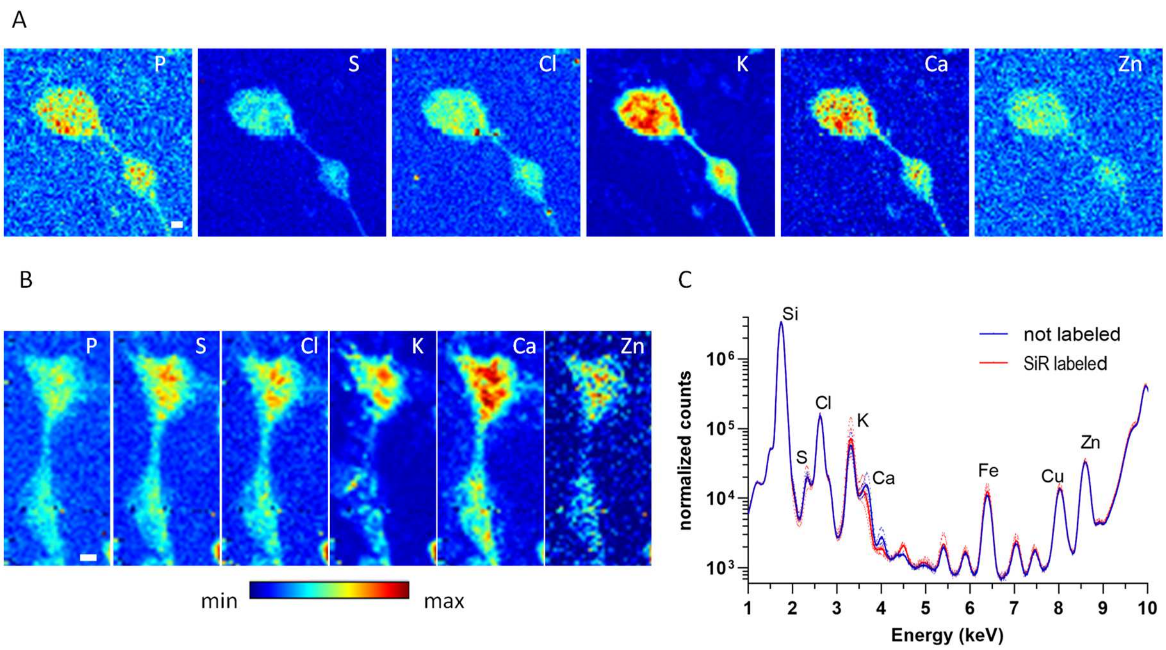

Fig. 3. Comparison of the SXRF signal of neurons labeled with SiR fluorophores *vs* not labeled neurons. A) SXRF elemental maps from a growth cone labeled with SiR probes. B) SXRF elemental maps from a growth cone not labeled. C) SXRF spectra from different growth cones; Blue single points represent the SXRF spectra from five unlabeled growth cones, and the solid blue line the mean spectrum of these five single analyses. Red single points represent the SXRF spectra from eight SiR-labeled growth cones, and the solid red line the mean of them.

3.4. Preservation of cell morphology

The sample preparation protocol requires cryofixation and freeze-drying steps to avoid chemical fixation. We verified that cell morphology was well preserved at the level of synaptic structures using scanning electron microscopy (SEM). Samples prepared following the protocol developed for SXRF imaging, i.e. after cryofixation and freeze-drying under mild conditions, were observed by SEM without any additional preparation steps (Fig. 4). Morphological preservation is of excellent quality, especially on the thinner parts of the cell structures, the dendrites and dendritic spines (Fig. 4B and 4C). Minor damage to the morphological structure is observed on the thickest regions of the sample with a relatively flat shape of the soma and some broken branches of dendrites extending from the cell body (Fig. 4A). This is easily explained, the finest structures remain the best preserved because they are cryofixed more quickly and less affected by the collapse of the structure during freeze-drying. On the other hand, on the thicker parts, the structure presents some minor damage because cryofixation is a little slower and especially the shear stresses are more important between the much thicker cell body and the dendrites resulting sometimes in breaks. The preservation remains however suitable for SXRF analysis. Overall, the cryofixation and freeze-drying protocol allows to preserve the cell morphology at the scale of the structures of interest, dendrites and dendritic spines.

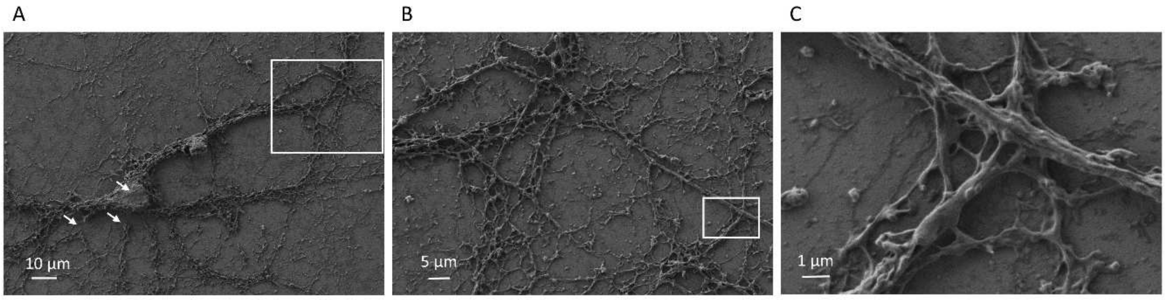

Fig. 4. Scanning electron microscopy of a neuron cultured on a SN membrane after cryofixation and freeze-drying. The freeze-dried sample was observed in SEM as prepared for SXRF analysis without any further processing steps. The sample shows an excellent morphological preservation as illustrated by SEM at different magnifications especially of the thinner structures. Minor alterations of the cell morphology are observed, indicated by arrows, with a relatively flat structure of the soma and breaks between the soma and some dendrites. (A) Soma and dendrites (x660). (B) Large and thin dendrites enlarged from the region framed in A (x1,500). (C) Thin dendrites at high magnification from the framed region in B (x10,000).

3.5. Limitations of the correlative imaging due to sample processing

With our protocol the morphology of cellular structures after freeze-drying is overall well preserved (Fig. 4) but slight differences between the images before and after freeze-drying are nevertheless observed. Freeze-drying is known to alter the cellular morphology at the nanoscale (Hempel et al., 2020). We could study morphological modifications by comparing the fluorescence of labeled proteins before and after freeze-drying (Fig. 5). Contrary to fluorescent proteins such as GFP, the fluorescence of inorganic dyes is maintained after freeze-drying (Roudeau et al., 2014). This is the case for SiR based molecules, their fluorescence can be observed by confocal microscopy after freeze-drying (Fig. 5C), although with a decreased intensity hampering to perform STED. We have used this property of SiR based fluorescent dyes to compare the distribution of tubulin fluorescence before and after freeze-drying showing for example a shrinkage from 1.1 µm to 0.7 µm in dendrite cross-sections (Fig. 5B and 5D). This shrinkage is most probably due to the effect of water loss by sublimation resulting in a partial collapse of the cellular architecture in freeze-dried cells compared to living cells. Structural shrinkage is well visible for example in the dendrites, but also in the F-actin rich region in the growth cone. This shrinkage however does not influence notably the compartmentalization of the proteins and of the elements in the subcellular compartments (Fig. 5E).

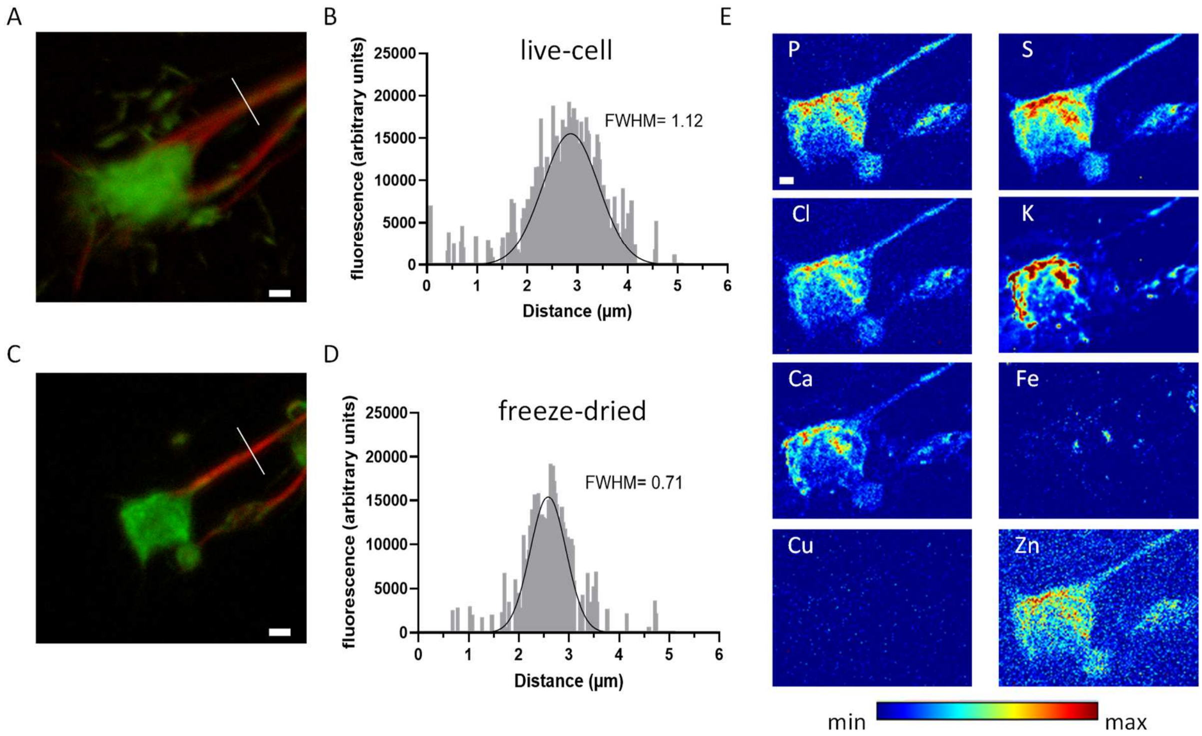

Fig. 5. Comparison of protein distributions before and after plunge-freezing/freeze-drying. (A) Live-cell confocal microscopy of a growth cone from a DIV3 neuron labeled with SiR-tubulin and SiR-700-actin. (B) Plot profile of the fluorescence intensity of tubulin along the white line shown in A. (C) Confocal microscopy of SiR-tubulin and SiR-700-actin in the same growth cone after plunge-freezing and freeze-drying. (D) Plot profile of the fluorescence intensity of tubulin along the white line shown in C. (E) SXRF images of chemical elements (P, S, Cl, K, Ca, Fe, Cu and Zn) from the growth cone in shown in C, after plunge freezing and freeze-drying. Color scale bar: min-max values. Scale bars: A) and C) 2 µm, E) 1 µm.

It may also be possible that morphological modifications between living neurons and plunge-frozen/freeze-dried ones are the consequence of changes in cellular structures during the elapsed time between STED observation and the plunge-freezing, especially with highly dynamic structures such as growth cones. In our study, this eventuality could be limited by the labeling with SiR-tubulin and SiR700-actin that are based on cytoskeleton stabilizing molecules that will slow down the dynamic changes of the cellular structures.

3.6. Correlative imaging in sub-synaptic compartments

One of the main objectives of the development of correlative imaging of proteins and metals at high spatial resolution is to be able to study biological structures of submicrometer size, with in the case of neurons a particular interest for the synaptic compartments. We present an example of such achievement in Fig. 6. Primary rat hippocampal neurons were transfected for expression of Xph20-eGFP that binds the post-synaptic density protein PSD-95 (Rimbault et al., 2021). At DIV15 neurons were labeled with SiR-tubulin and observed by confocal and STED microscopy (Fig. 6A and 6B). Postsynaptic compartments identified by STED microscopy on living neurons, such as illustrated in Fig. 6C, were subsequently observed by SXRF imaging at the APS Bionanoprobe on freeze dried samples (Fig. 6D). The arrows in Fig. 6D show the position of a protrusion along the microtubule branching, which corresponds to the position of the fluorescently labeled PSD-95 in Fig. 6C. This image suggest that the post-synaptic compartment of hippocampal neurons contains P, S, K and Zn, sharing a similar distribution, while Cl and Fe display a different distribution compared to the other elements. Calcium distribution is also similar to those of P, S, K and Zn but with a lower intensity in the analyzed post-synaptic compartments compared to other regions along the dendrites that contain higher Ca levels. A similar example is illustrated in Fig. 7 showing the partial co-localization of chemical elements such as P, S, K, Ca, and Zn with the position of PSD-95 (Fig. 7D). In this example again, Cl and Fe have a different distribution than the previously mentioned elements. Very interestingly, Cu also appears mainly outside the PSD-95 labeled regions. Copper is an important biological relevant metal potentially involved in neuronal signaling, differentiation and synaptic shaping (D'Ambrosi et al., 2015; Hatori et al., 2016; Domart et al., 2020). Cu is a very difficult element to detect even with spectro-imaging techniques of ultimate sensitivity such as SXRF due to its lower concentrations in biological systems compared for example to Fe or Zn (Domart et al., 2020; Carmona et al., 2022).

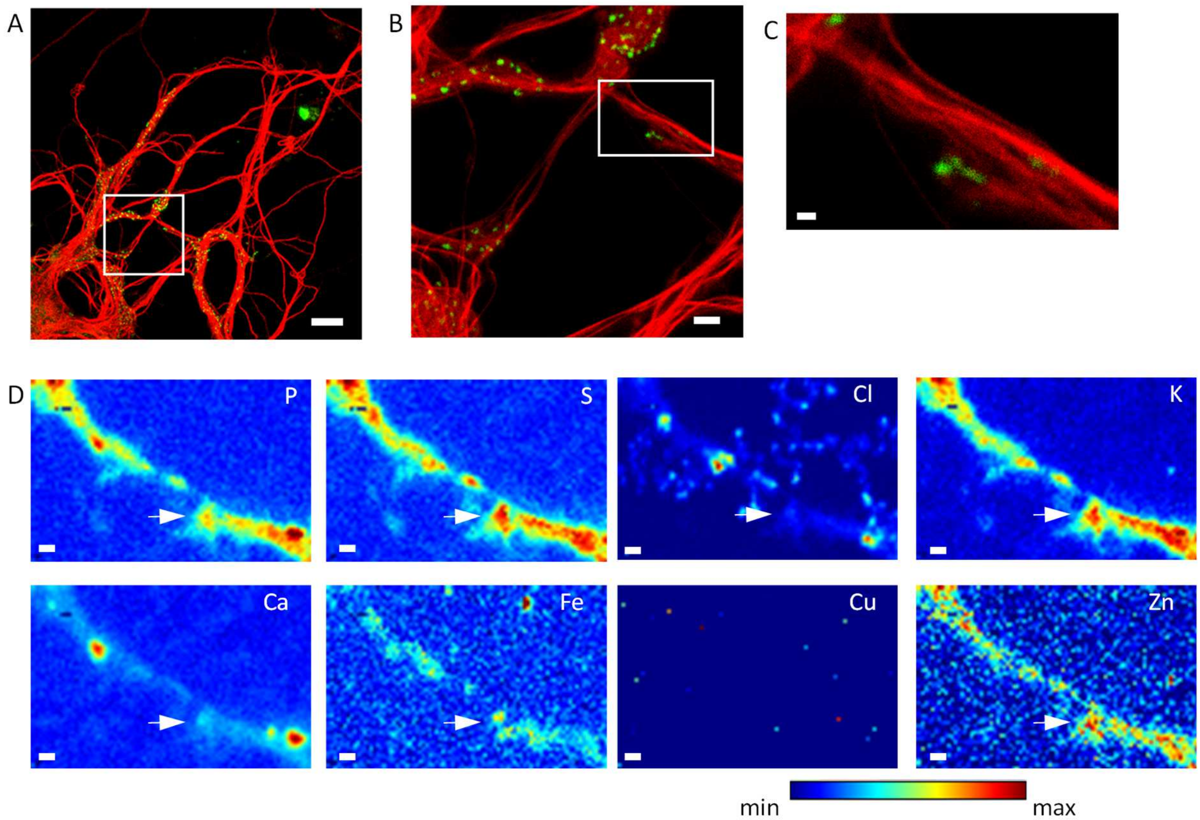

Fig. 6. Correlation of STED microscopy and nano-SXRF images obtained at the BioNanoprobe (APS). (A) Confocal microscopy view of tubulin (red, labeled with SiR-tubulin) and PSD-95 (green, labeled with Xph20-eGFP) a marker of the post-synaptic compartments, in living cells. (B) Live-cell STED microscopy images of tubulin (red) and PSD-95 (green) corresponding to the white square region in A. (C) Zoom in the region of the white square shown in B, corresponding to the sample's area imaged by SXRF. (D)

SXRF images of chemical elements (P, S, Cl, K, Ca, Fe and Zn) from the region in the white square shown in C, after plunge freezing and freeze-drying. Color scale bar: min-max values. Scale bars: (A) 10 µm, (B) 2 µm, (C, D) 0.5 µm.

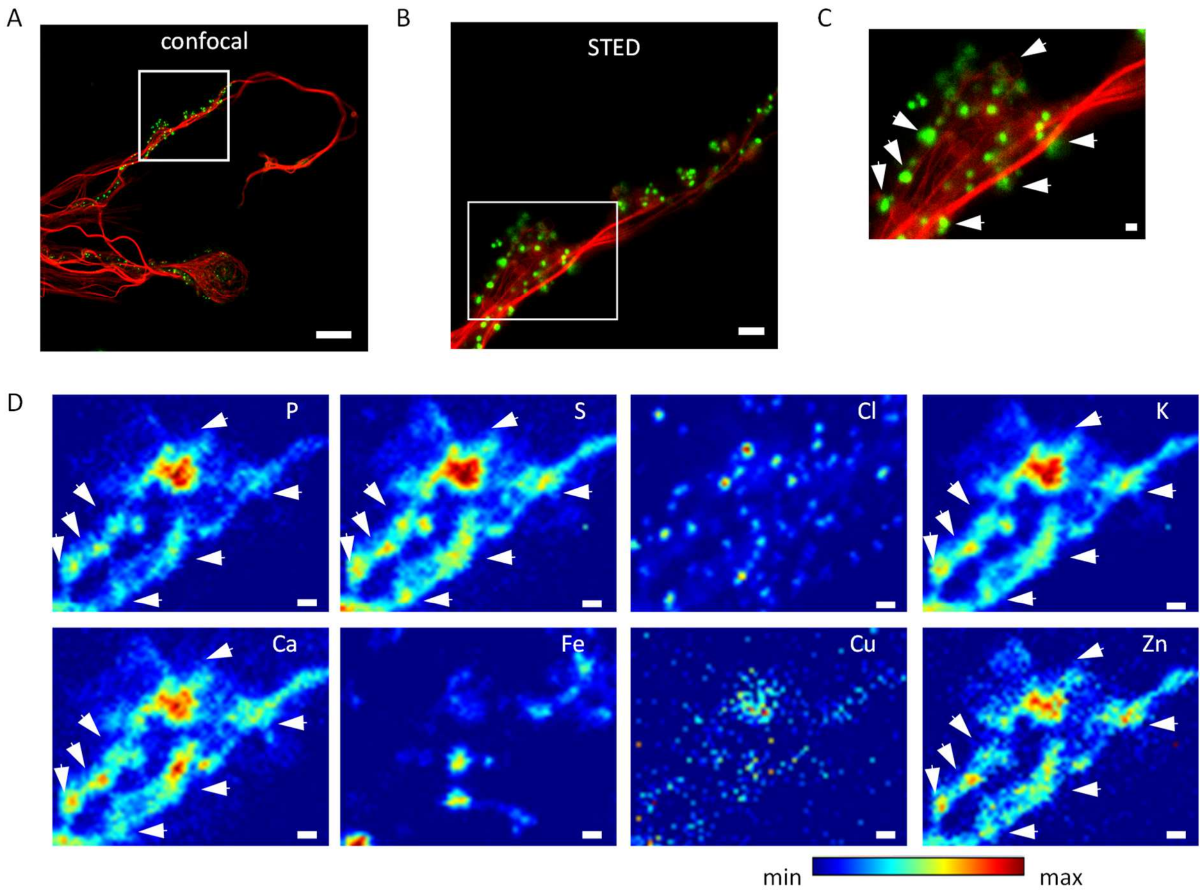

Fig. 7. Correlation of STED microscopy and nano-SXRF images obtained at the BioNanoprobe (APS). (A) Confocal microscopy view of tubulin (red, labeled with SiR-tubulin) and PSD-95 (green, labeled with Xph20-eGFP), in living cells. (B) Live-cell STED microscopy images of tubulin (red) and PSD-95 (green) corresponding to the white square region in A. (C) Zoom in the region of the white square shown in B, corresponding to the sample's area imaged by SXRF. (D) SXRF images of chemical elements (P, S, Cl, K, Ca, Fe, Cu and Zn) from the region in the white square shown in C, after plunge freezing and freeze-drying. The arrows indicate the location of some elements following the same distribution pattern as the PSD-95 shown in C. Color scale bar: min-max values. Scale bars: (A) 10 µm, (B) 2 µm, (C, D) 0.5 µm.

4. Conclusion

Correlative imaging of metals and proteins in synaptic compartments will provide a better understanding of the physiological role of metals in neuronal processes. Such investigations require adapted observation and preparation protocols. We have experimentally validated the methodological approach of correlating STED and SXRF images obtained with a similar spatial resolution, around 40 nm. The chosen imaging sequence consists in first observing the living cells by STED, then imaging by

SXRF once plunge-frozen and freeze-dried. The established protocol allows correlative imaging at high spatial resolution but can still be improved. The most limiting step of the protocol is the freeze-drying which can cause shrinkage of cell structures. A way to limit such effects would be to skip the freeze-drying step and image directly the samples in their frozen hydrated sate using SXRF in cryogenic conditions, after live-STED microscopy. Ideally, in the future, a fully cryogenic correlative mode of cryo-fluorescence microcopy and cryo-SXRF would allow to observe the exact same cellular structures.

Declaration of competing Interest

None.

Credit Author Statement

Richard Ortega: Conceptualization, Funding acquisition, Investigation, Writing- Original draft preparation, Writing - Review & Editing. **Stephane Roudeau**: Investigation, Formal analysis, Writing - Review & Editing. **Asuncion Carmona**: Project administration, Methodology, Investigation, Formal analysis, Writing- Original draft preparation, Writing - Review & Editing.

Acknowledgements

This project was supported by a grant from Centre National de la Recherche Scientifique (CNRS) through the MITI interdisciplinary program. We are very grateful do Dr. Daniel Choquet of the Interdisciplinary Institute for Neuroscience (IINS) for his support and advice, and to Dr. Florelle Domart for her initial contribution to the project. SXRF experiments were performed on beamline ID16A at the European Synchrotron Radiation Facility (ESRF), Grenoble, France. We are deeply grateful to Dr. Peter Cloetens (ESRF) for the fruitful collaboration. Use of the Advanced Photon Source, an Office of Science User Facility operated for the U.S. Department of Energy (DOE) Office of Science by Argonne National Laboratory, was supported by the U.S. DOE under Contract No. DE-AC02-06CH11357. Our thanks to Dr. Si Chen (APS) for assistance in using the BioNanoprobe beamline. We would like to thank the Cell Biology Facility from IINS, especially Emeline Verdier and Natacha Retailleau for molecular and cellular tool productions and general cell biology activity management. We thank Dr. Matthieu Sainlos (IINS) for providing the xph20-eGFP construct. The SEM, STED and confocal microscopy were done in the Bordeaux Imaging Center, a service unit of the CNRS-INSERM and Bordeaux University, member of the national infrastructure France BioImaging. We are very thankful to Dr. Etienne Gontier for assistance with SEM.

References

Carmona A, Chen S, Domart F, Choquet D, Ortega R, 2022. Imaging the structural organization of chemical elements in growth cones of developing hippocampal neurons. Metallomics. 14, mfab073. doi: 10.1093/mtomcs/mfab073.

Chen S, Deng J, Yuan Y, Flachenecker C, Mak R, Hornberger B, Jin Q, Shu D, Lai B, Maser J, Roehrig C, Paunesku T, Gleber SC, Vine DJ, Finney L, VonOsinski J, Bolbat M, Spink I, Chen Z, Steele J, Trapp D, Irwin J, Feser M, Snyder E, Brister K, Jacobsen C, Woloschak G, Vogt S, 2014. The Bionanoprobe: hard X-ray fluorescence nanoprobe with cryogenic capabilities. J. Synchrotron Rad. 21, 66-75. doi: 10.1107/S1600577513029676.

Choquet D, Sainlos M, Sibarita JB., 2021. Advanced imaging and labelling methods to decipher brain cell organization and function. Nat Rev Neurosci. 22, 237-255. doi: 10.1038/s41583-021-00441-z.

D'Ambrosi N, Rossi L., 2015. Copper at synapse: Release, binding and modulation of neurotransmission. Neurochem Int., 90, 36-45. doi: 10.1016/j.neuint.2015.07.006.

Da Silva JC, Pacureanu A, Yang Y, Bohic S, Morawe C, Barrett R, Cloetens P, 2017. Efficient concentration of high-energy x-rays for diffraction-limited imaging resolution. Optica 4, 492-495. https://doi.org/10.1364/OPTICA.4.000492

Domart F, Cloetens P, Roudeau S, Carmona A, Verdier E, Choquet D, Ortega R, 2020. Correlating STED and synchrotron XRF nano-imaging unveils cosegregation of metals and cytoskeleton proteins in dendrites. Elife, 9:e62334. doi: 10.7554/eLife.62334.

Ellison G, Hollings A.L., Hackett M.J., 2022. A review of the “metallome” within neurons and glia, as revealed by elemental mapping of brain tissue, BBA Advances, 2, 10003. https://doi.org/10.1016/j.bbadva.2021.100038.

Finnegan ME, Visanji NP, Romero-Canelon I, House E, Rajan S, Mosselmans JFW, Hazrati LN, Dobson J, Collingwood JF., 2019. Synchrotron XRF imaging of Alzheimer's disease basal ganglia reveals linear dependence of high-field magnetic resonance microscopy on tissue iron concentration. J Neurosci Methods. 319, 28-39. doi: 10.1016/j.jneumeth.2019.03.002.

Hatori Y, Yan Y, Schmidt K, Furukawa E, Hasan NM, Yang N, Liu CN, Sockanathan S, Lutsenko S., 2016. Neuronal differentiation is associated with a redox-regulated increase of copper flow to the secretory pathway. Nat Commun. 7, 10640. doi: 10.1038/ncomms10640.

Hempel C, Kapishnikov S, Perez-Berna AJ, Werner S, Guttmann P, Pereiro E, Qvortrup K, Andresen TL., 2020. The need to freeze-dehydration during specimen preparation for electron microscopy collapses the endothelial glycocalyx regardless of fixation method. Microcirculation 27, e12643. doi: 10.1111/micc.12643.

Jin Q, Paunesku T, Lai B, Gleber SC, Chen SI, Finney L, Vine D, Vogt S, Woloschak G, Jacobsen C., 2017. Preserving elemental content in adherent mammalian cells for analysis by synchrotron-based x-ray fluorescence microscopy. J Microsc. 265, 81-93. doi: 10.1111/jmi.12466

Kaech S, Banker G., 2006. Culturing hippocampal neurons. Nat Protoc. 1, 2406-15. doi: 10.1038/nprot.2006.356.

Li Y, Almassalha LM, Chandler JE, Zhou X, Stypula-Cyrus YE, Hujsak KA, Roth EW, Bleher R, Subramanian H, Szleifer I, Dravid VP, Backman V., 2017. The effects of chemical fixation on the cellular nanostructure. Exp Cell Res. 358, 253-259. doi: 10.1016/j.yexcr.2017.06.022.

Lukinavičius G, Reymond L, Umezawa K, Sallin O, D’Este E, Göttfert F, Ta H, Hell SW, Urano Y, Johnsson K, D'Este E, 2016. Fluorogenic probes for multicolor imaging in living cells. J. Am. Chem. Soc. 138, 9365–9368. https://doi.org/10.1021/jacs.6b04782

Perrin L, Carmona A, Roudeau S, Ortega R, 2015. Evaluation of sample preparation methods for single cell quantitative elemental imaging using proton or synchrotron radiation focused beams. J. Anal. At. Spectrom. 30, 2525-2532. doi: 10.1039/C5JA00303B

Perrin L, Roudeau S, Carmona A, Domart F, Petersen JD, Bohic S, Yang Y, Cloetens P, Ortega R., 2017. Zinc and copper effects on stability of tubulin and actin networks in dendrites and spines of hippocampal neurons. ACS Chem Neurosci., 8, 1490-99. doi:10.1021/acschemneuro.6b00452.

Rimbault C., Breillat C., Compans B., Toulmé E., Vicente F. N., Fernandez-Monreal M., Mascalchi P., Genuer C., Puente-Muñoz V., Gauthereau I., Hosy E., Giannone G., Chamma I., Mackereth C. D., Poujol C., Choquet D., Sainlos M., 2021. Engineering paralog-specific PSD-95 synthetic binders as potent and minimally invasive imaging probes. bioRxiv, 2021.04.07.438431. doi: https://doi.org/10.1101/2021.04.07.438431

Roudeau S, Carmona A, Perrin L, Ortega R., 2014. Correlative organelle fluorescence microscopy and synchrotron X-ray chemical element imaging in single cells. Anal. Bioanal. Chem. 406, 6979-91. doi: 10.1007/s00216-014-8004-4.

Solé V.A., Papillon E., Cotte M., Walter P., Susini J., 2007. A multiplatform code for the analysis of energy-dispersive X-ray fluorescence spectra. Spectrochim. Acta B 62, 63–68. https://doi.org/10.1016/j.sab.2006.12.002

Vogt S., 2003. MAPS: a set of software tools for analysis and visualization of 3D X-ray fluorescence data sets. Journal de Physique IV, 104, 635–638. doi: 10.1051/jp4:20030160.

Wandt VK, Winkelbeiner N, Bornhorst J, Witt B, Raschke S, Simon L, Ebert F, Kipp AP, Schwerdtle T., 2021. A matter of concern - Trace element dyshomeostasis and genomic stability in neurons. Redox Biol. 41, 101877. doi: 10.1016/j.redox.2021.101877.

White A.R., 2017. Metals in the Brain, Neuromethods (NM, volume 124), Springer, New York USA. https://doi.org/10.1007/978-1-4939-6918-0

Correlative nano-imaging of proteins and metals